ISSN (Print) 1226-1750
ISSN (Online) 2233-6656
Journal of Magnetics 30(4), 575-581 (2025) https://doi.org/10.4283/JMAG.2025.30.4.575

Improved Inverse Preisach Model for Modeling Hysteresis Properties of Grain-Oriented Silicon Steel

Long Chen[1,2], Long Tan[1], Tong Ben[2]*, Libing Jing[1], and Wenguang Ke[1]

[1]*College of Electrical Engineering and New Energy, China Three Gorges University, Yichang 443002, Hubei Province, China*
[2]*Hubei Provincial Engineering Technology Research Center for Power Transmission Line, China Three Gorges University, Yichang, 443002, China*

(Received 29 May 2025, Received in final form 15 September 2025, Accepted 15 September 2025)

Accurate and meticulous modeling of the hysteresis loops displayed by electrical steels under complex waveforms with diverse magnetization intensities is of paramount importance for achieving the utmost excellence in electrical equipment design.In particular, inverse hysteresis models are preferable in FEM for deriving magnetic field values from vector potential to reduce iterations. However, the prevailing inverse Preisach models, which are grounded in the inverse Everett function, fall short in elucidating the intrinsic physical nature of hysteresis phenomena associated with the magnetization process. Moreover, their generalized moving adaptations entail substantial computational costs when integrated with Finite Element Method (FEM) software. This study presents a generalized, analytically derived inverse Preisach model.It characterizes an analytical Everett function for the irreversible component while explicitly incorporating both hysteresis dependence on magnetization state and reversible contributions. The resulting model guarantees accuracy for symmetric and asymmetric minor loop simulations and enables straightforward FEM implementation. Validation with B30P105 grain-oriented silicon steel measurements across varied excitation levels confirms model accuracy, with computational performance benchmarked against conventional approaches.

Keywords : hysteresis model, grain-oriented silicon steel, transformers, Finite element Method (FEM)

1. Introduction

Precise characterization of hysteresis behavior in electrical steel sheets critically enables magnetic field analysis and efficiency optimization in key electromagnetic devices including motors and transformers [1].

Previous research has put forward a variety of approaches for hysteresis modeling, including the Jiles - Atherton model, the Preisach model, the energetic model, and the Stoner - Wohlfarth model, among others [2-4]. Among these, the classic Preisach model stands out as one of the most widely used. Rooted in the physical assumptions of magnetic dipoles, it offers a relatively high level of simulation accuracy.

During the design of electrical equipment, the magnetic vector potential A is commonly employed to analyze magnetic field distribution through finite element analysis (FEA). Under such circumstances, employing the forward Preisach model—which relies on magnetic field strength H to determine magnetic flux density B—often results in a higher number of iterations. Consequently, the inverse Preisach model emerges as a more suitable alternative for this application.

Various inverse Preisach models have recently been developed to improve FEM calculation speed [5, 6]. To avoid solving double integrals in the Preisach model, an Everett function-based inverse Preisach formulation has been introduced in literature [7]. To address the requirement of maintaining mathematical rigor in the distribution function, researchers have subsequently developed a modified inversion approach using a switch hysteresis operator-based framework [8]. However, the above models can only deal with a magnetization-independent process. In that situation, the congruency property of the inverse model is retained, which is inconsistent with the nature of the magnetization process for ferromagnetic materials, resulting in an error when simulating the minor loops caused by PWM excitations. The magnetic polarization behavior in materials is typically characterized by two distinct mechanisms: reversible magnetization and non-reversible (hysteretic) magnetization processes. As per the moving Preisach model framework, the model's congruency requirement can be strategically relaxed through the integration of a feedback parameter [9].

*Corresponding author: Tel: +86-18522089362
e-mail: chenlong@ctgu.edu.cn

Nevertheless, the traditional moving model is an H-based forward Preisach model, which is not convenient in FEA. In [10], a generalized inverse Preisach model was proposed in 2020 to consider the reversible and magnetization-dependent components, achieving accurate simulations of the minor loops. Although the model mentioned above can reduce the times of the iterations as it is a B-based inverse model, it still has an enormous computational burden when incorporated with the FEM program, as the Everett function used in the model is discrete. The discrete Everett function can result in bad convergence performance and need a large memory space, which will increase the total execution time of the whole FEA process. Thus, a generalized inverse Preisach model with an analytical Everett function needs to be further studied. To the best of our knowledge, the computational efficiency of the model can be improved by applying a closed-form Everett function [6, 11]. However, none of the abovementioned methods considered the feedback coefficient in the magnetization process.

This study develops a generalized analytical inverse Preisach formulation. The non-reversible magnetic polarization behavior is characterized using an analytical Everett function framework. Reversible components coupled with magnetization-dependent effects are integrated into the analytical inversion model through temporal discretization of the effective field parameters. Model performance is rigorously validated by contrasting computed hysteresis curves with experimental measurements obtained from B30P105 grain-oriented electrical steel specimens.

2. The classical Preisach Model

The foundational Preisach model posits that ferromagnetic materials comprise a vast ensemble of magnetic hysteresis elements, each exhibiting characteristic rectangular-shaped response curves. As illustrated in Fig. 1(a), the model defines two critical switching thresholds (α and β) governing the ascending and descending transitions of each hysteresis element. In this framework, H represents the externally applied magnetic field intensity, while γ denotes the binary output state (+1 or -1) of the individual hysteresis operator. The macroscopic magnetization behavior described by the classical Preisach model can be mathematically expressed as:

$$M(H) = \iint_{\partial \geq \beta} \mu(\alpha, \beta) \gamma_{\alpha\beta}(H) d\alpha d\beta \tag{1}$$

$$B = \mu_0 (H + M(H)) \tag{2}$$

Where $\mu(\alpha, \beta)$ is the distribution function of the Preisach hysteresis operator; $\gamma_{\alpha\beta}(H)$ is the hysteresis operator.

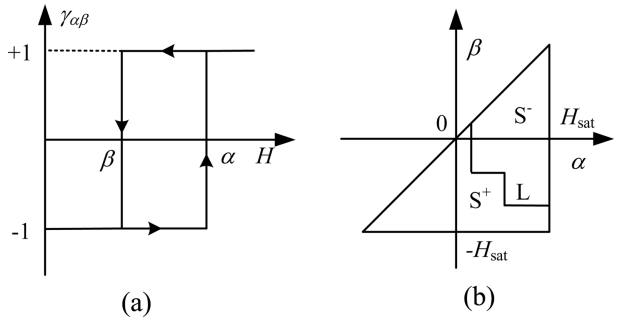

Fig. 1. (a) Preisach switched hysteresis operator. (b) Typical Preisach diagram.

The output of the classical Preisach model can be solved according to the diagram in Fig. 1(b), where the hysteresis operator corresponds to the points in the triangular region $\alpha \geq \beta$. The integration region S is divided into two parts, the value of the hysteresis operator is +1 in the S+ region, and the value of the operator is -1 in the S-region.

From (1), the classic Preisach model contains a complex distribution function dual integral operation, which will lead to the model with a cumbersome parameter identification process and long calculation time. To avoid the double integral problem, an Everett function $E(\alpha, \beta)$ is introduced into the classical Preisach model, and (1) can be changed to:

$$M(H) = \begin{cases} M_K - 2E(H_K, H) & \text{(downward magnetization)} \\ M_k + 2E(H, H_k) & \text{(upward magnetization)} \end{cases} \tag{3}$$

Here, H_k denotes the magnetic intensity at the final reversal point. However, when using (3) to incorporate with the FEM, a large discrete matrix will generate, and it is computationally very expensive.

3. Generalized analytical inverse Preisach model

3.1. The analytical Everett function in the forward Preisach model

In the implementation of the conventional Preisach framework, the Everett function formulation can be mathematically represented using Lorentzian distributions [6,12]. Parameter calibration for these methodologies becomes computationally intensive due to the large number of undetermined coefficients. To address this complexity, an analytical Everett function formulation is developed using hyperbolic tangent basis functions:

$$E(\alpha,\beta) = a(\tanh(\frac{\alpha}{b}) - \tanh(\frac{\beta}{b}))^5 + c(\tanh(\frac{\alpha}{d}) - \tanh(\frac{\beta}{d}))^4 + e\alpha\beta \quad (4)$$

Where α to e are the unknown parameters of the analytical Everett function. It can be found that the number of the parameters is vastly reduced, and the value of the Everett function can be determined from the descending branch of the concentric hysteresis loops as:

$$E(\alpha,\beta) = \frac{M_{\alpha\alpha} - M_{\alpha\beta}}{2} \quad (5)$$

Where $M_{\alpha\alpha}$ is the peak value of magnetic flux density in concentric hysteresis loop, and $M_{\alpha\beta}$ corresponds to a point on the descending branch.

3.2. Generalized Inverse Preisach model in analytical form

The magnetic polarization process can be decomposed into two distinct components: an irreversible magnetization portion governed by hysteresis mechanisms, and a reversible magnetization portion associated with elastic deformation effects. While the classical Preisach framework is inherently limited to modeling the irreversible component through its hysteresis operator formalism, the reversible contribution requires separate characterization using the concept of reversible magnetic susceptibility:

$$M(H) = M_{\text{irr}}(H) + M_{\text{rev}}(H) \quad (6)$$

Where M_{irr} is the irreversible magnetization, and M_{rev} is the reversible magnetization.

The reversible magnetization exhibits exclusive dependence on instantaneous magnetic state, with its contribution being quantifiable through the parameter of reversible magnetic susceptibility. Notably, the hysteresis curve demonstrates distinct slope characteristics on either side of the magnetic reversal inflection point. This asymmetry stems from the system's complete reversibility of magnetic response following directional changes in the applied field, particularly after traversing the critical reversal threshold. Consequently, the reversible susceptibility coefficient (χ_{rev}) can be experimentally determined by evaluating the dM/dH gradient at the inflection regions of concentric hysteresis loops. Upon obtaining this calibration parameter, the reversible magnetization component is mathematically expressed as:

$$M_{\text{rev}}(H) = \int_0^H \chi_{\text{rev}}(H) dH \quad (7)$$

In the simulation of the electric field under different media, a single neural network is trained to find the solution, where the partial differential equation's form remains constant by adjusting various magnetic permeabilities.

Within the framework of the moving Preisach model, magnetization-dependent feedback mechanisms are introduced to mitigate the rigid congruency constraints inherent in classical formulations. This enhanced model incorporates an adjusted magnetic field parameter H that accounts for dynamic magnetization effects, with its mathematical representation formulated as:

$$H_{\text{e}} = H + KM \quad (8)$$

Where H_{e} is the adjusted magnetic intensity parameter, and K is the feedback coefficient. The feedback coefficient can be obtained by the following formula [10]:

$$K = \frac{M_{\text{e}} - M}{\chi M} \quad (9)$$

In this context, the term M_{e} corresponds to the experimentally measured magnetization, whereas M denotes the corresponding value predicted by the classical Preisach model formulation. The parameter χ quantifies the intrinsic magnetic susceptibility inherent to the principal hysteresis trajectory.

To obtain an efficient inverse form of the above model, a time-step difference on the magnetic field strength H is employed for calculating the input from the output, with the following formulation:

$$H_{i+1} = H_i + \frac{B_{i+1} - B_i}{(\text{d}B/\text{d}H)_i} \quad (10)$$

In this context, the parameter H_i represents the instantaneous applied field intensity, whereas H_{i+1} corresponds to the subsequent field magnitude determined in the following iterative step. The term (dB/dH)$_i$ denotes the flux density gradient of B_i with respect to the prevailing field intensity H_i at the current stage.

Computing the first-order derivative of equation (2), dB/dH can be obtained:

$$\frac{\text{d}B}{\text{d}H} = \mu_0(1 + \frac{\text{d}M}{\text{d}H}) \quad (11)$$

To incorporate magnetization feedback effects, the effective field parameter is redefined in terms of the nominal applied field intensity. This necessitates applying the following mathematical adjustment to the differential susceptibility term:

$$\frac{\text{d}M}{\text{d}H} = \frac{\text{d}M}{\text{d}H_{\text{e}}} \frac{\text{d}H_{\text{e}}}{\text{d}H} \quad (12)$$

Taking the first-order derivative of (8), dH_e/dH can be obtained.

$$\frac{dH_e}{dH} = 1 + K\frac{dM}{dH} \tag{13}$$

By combining (11), (12), and (13), it can be obtained:

$$\frac{dB}{dH} = \mu_0\left(1 + \frac{\frac{dM}{dH_e}}{1 - K\frac{dM}{dH_e}}\right) \tag{14}$$

Taking the first order derivative of (6), dM/dH_e can be obtained by

$$\frac{dM}{dH_e} = \frac{dM_{irr}}{dH_e} + \frac{dM_{rev}}{dH_e} \tag{15}$$

where dM_{rev}/dH_e can be obtained from the (7), the dM_{irr}/dH_e can be obtained from the (3) and (4), expressed as:

$$\frac{dM_{irr}}{dH_e} = \begin{cases} 2\left[\begin{array}{l}\frac{5a}{b}(\tanh(\frac{h}{b}) - \tanh(\frac{h_k}{b})^4)(1-\tanh^2(\frac{h}{b})) \\ +\frac{4c}{d}(\tanh(\frac{h}{d}) - \tanh(\frac{h_k}{d})^4(1-\tanh^2(\frac{h}{d})) + eh_k\end{array}\right] & H > H_k \\ -2\left[\begin{array}{l}\frac{5a}{b}(\tanh(\frac{h_k}{b}) - \tanh(\frac{h}{b})^4)(\tanh^2(\frac{h}{b}) - 1) \\ +\frac{4c}{d}(\tanh(\frac{h_k}{d}) - \tanh(\frac{h}{d})^4(\tanh^2(\frac{h}{d}) - 1) + eh_k\end{array}\right] & H \le H_k \end{cases} \tag{16}$$

Here, H_k denotes the field magnitude at the preceding reversal threshold. For $H \le H_k$, the system undergoes demagnetization processes corresponding to downward magnetic polarization; conversely, when $H > H_k$, upward magnetization enhancement occurs. The schematic diagram of the implemented inverse Preisach modeling framework is illustrated in Fig. 2.

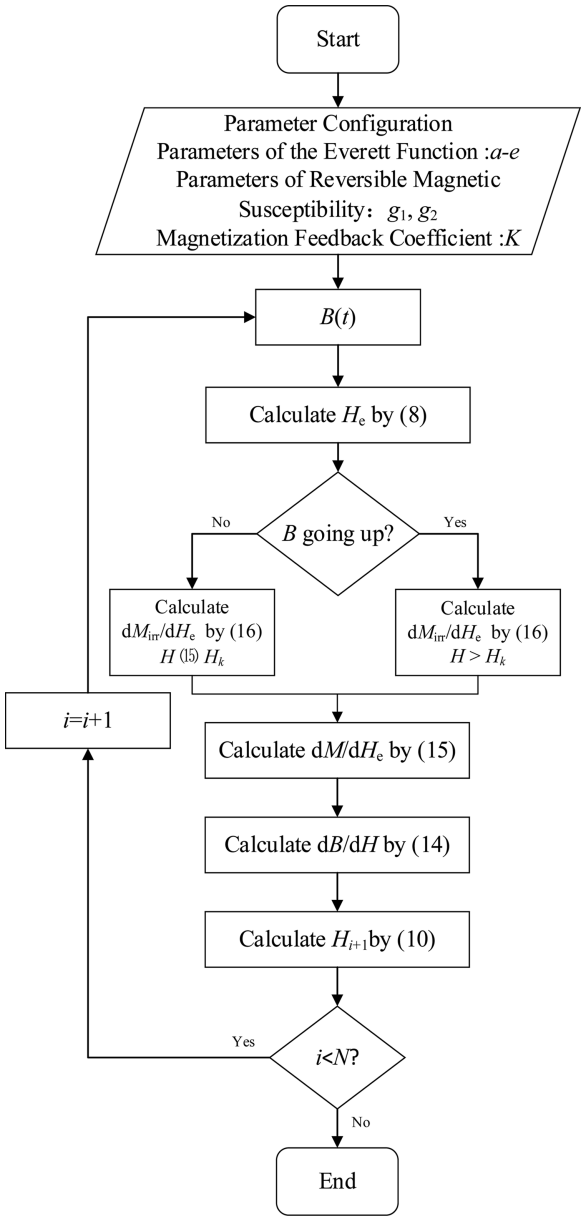

Fig. 2. Flow chart of the proposed inverse Preisach model.

4. Results and Discussion

4.1. Parameters identifications of the model

The irreversible and reversible components of the Preisach model were characterized through quasi-static measurements of magnetic hysteresis loops performed on B30P105 electrical steel using a ring-core experimental configuration, as depicted in Fig. 3.

To characterize the irreversible and reversible components within the Preisach framework, quasistatic magnetic hysteresis measurements were conducted on B30P105 electrical steel samples using a toroidal core measurement configuration (Fig. 2). Corresponding hysteresis curves were acquired under 5 Hz sinusoidal excitations across varying peak flux density levels, with results presented in Fig. 4(a). For validation of minor loop simulation capabilities, additional measurements under 5 Hz PWM excitation waveforms (containing fundamental frequency components) were performed, with corresponding data shown in Fig. 4(b).

To obtain the unknown parameters of the analytical Everett function, it is necessary to obtain the reversible magnetization of the hysteresis loop. The reversible magnetic susceptibility calculated value is fitted by an exponential function with parameters as:

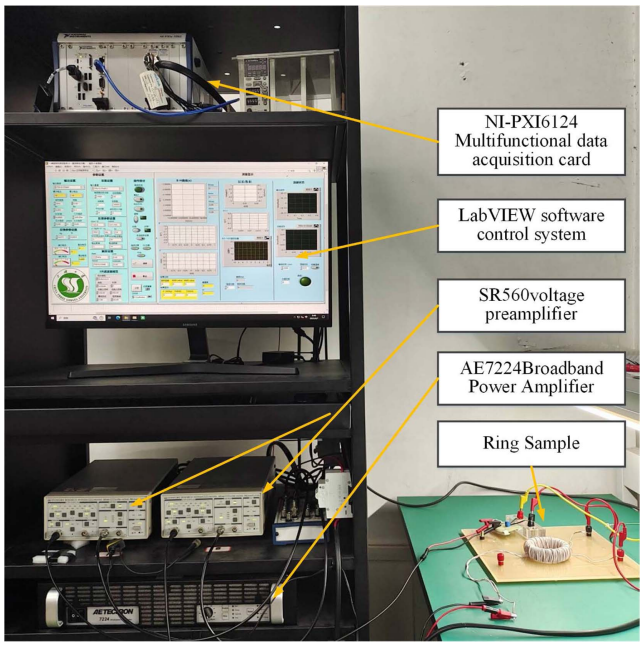

Fig. 3. (Color online) Experimental setup for measuring hysteresis loops of B30P105.

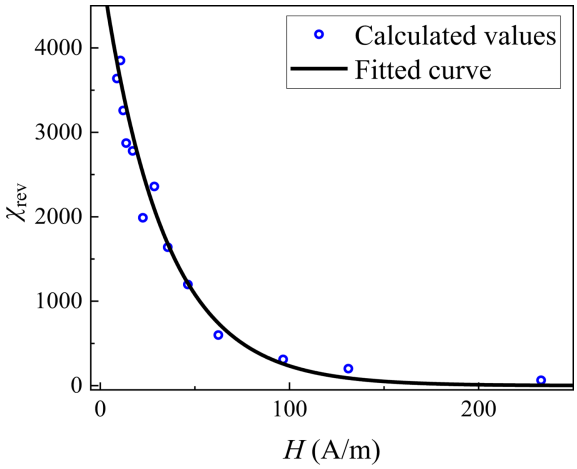

Fig. 5. (Color online) The reversible magnetic susceptibility of the B30P105 electrical steel sheet.

Table 1. Parameters of the analytical Everett function.

a	b	c	d	e
18227	12.33	33934	15.036	-1.76

$$\chi_{rev}(H) = g_1 e^{g_2|H|} \tag{17}$$

Where g_1 and g_2 are the parameters to be determined, the fitting results are shown in Fig. 5, and the equation parameter values g_1 is 5026 and g_2 is -0.0307.

The irreversible component of the magnetic hysteresis characteristics is isolated through experimental measurement of loop trajectories, followed by mathematical extraction of the reversible portion according to the formulation:

$$M_{irr} = M_{meas}(H) - M_{rev}(H) \tag{18}$$

Based on the irreversible part of the quasi-static hysteresis loops shown in Fig. 6, the calculated value of the Everett function can be obtained through (5), and the fitness parameters of (4) are determined and shown in Table 1. The feedback coefficient K can be obtained by calculating the average value of the feedback coefficient at the negative saturation point of the descending branch of different loops [10]. In this paper, the loops of B_p=0.4 T, 0.8 T, and 1.2 T are used to identify the value and identified as -5.694×10^{-7}.

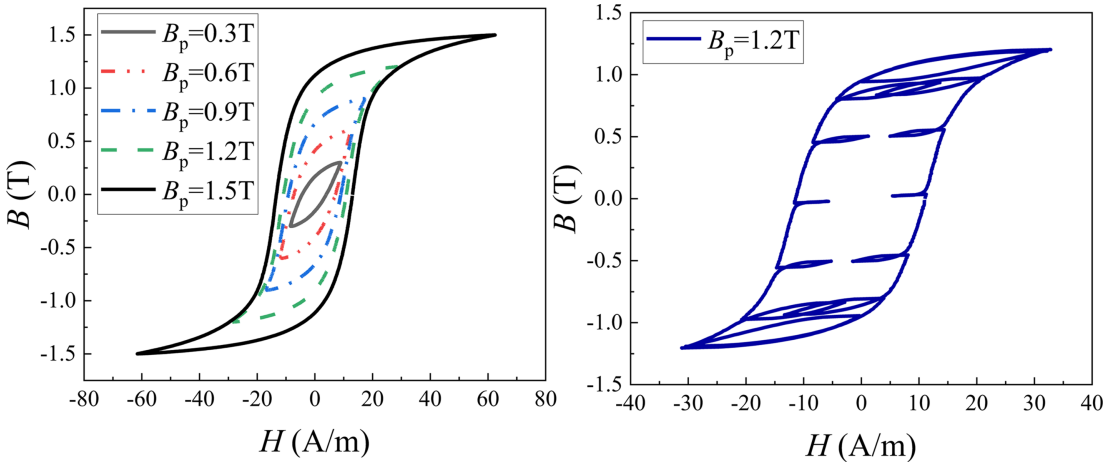

Fig. 4. (Color online) The quasi-static hysteresis loops of silicon steel B30P105: (a) The hysteresis loops under sinusoidal excitation. (b) The hysteresis loops under PWM excitation.

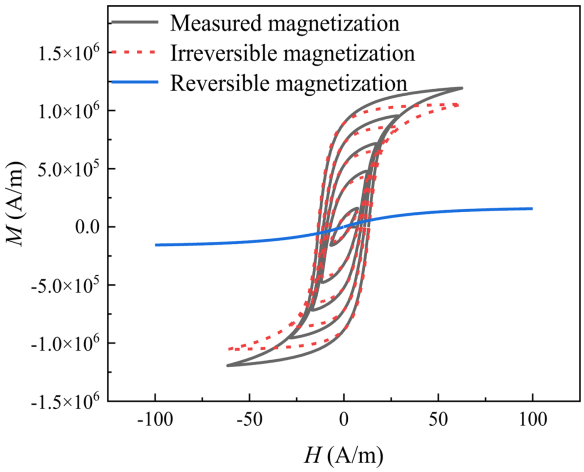

Fig. 6. (Color online) The magnetization of the B30P105 electrical steel sheet.

4.2. Verification of the simulated results

To validate the performance of the developed framework, the simulated hysteresis characteristics generated by the enhanced model under varying peak flux density conditions are benchmarked against laboratory-measured datasets. The Comparison of experimental and simulated hysteresis loops of B30P105 silicon steel sheet (The fundamental frequency is 5 Hz) is shown in Fig. 7. Fig. 7(a) illustrates the situation under sinusoidal conditions. Fig. 7(b) and (c) depict the cases under 30% third harmonic excitation with a harmonic phase angle of 190°and 0°, respectively. Fig. 7(d) presents the situation under PWM excitation with a duty cycle of 0.9.

It can be found that the most simulated loops are in good agreement with the measured ones, which can verify the model's ability to simulate the global hysteresis properties of the material. Because of the strong nonlinearity in high flux density levels, the dM/dH_e will cause an error even if the Everett function is fitted well, causing an error for the loops in relatively high magnetic flux density levels. In other words, this is mainly because under high magnetic flux density, a minor variation in the magnetic flux can induce significant changes in the magnetic field. Furthermore, the parameters of the analytical function are not mutually independent during the optimization process, making it difficult to accurately capture such nonlinear variations once the solution approaches its optimum. Due to the strong nonlinear adaptability and generalization capability, deep neural networks (DNNs) may be leveraged as a potential tool to address simulation inaccuracies under high magnetic flux

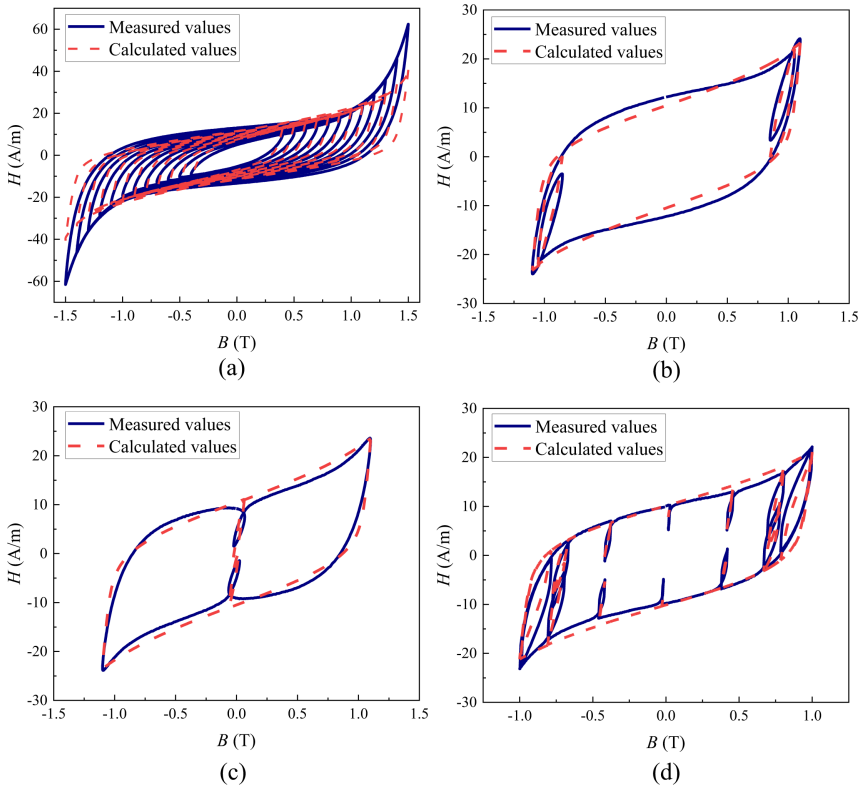

Fig. 7. (Color online) Comparison of experimental and simulated hysteresis loops of B30P105 silicon steel sheet (The fundamental frequency is 5 Hz): (a) Sinusoidal excitation. (b) 30% third harmonic excitation with harmonic phase angle 190°. (c) 30% third harmonic excitation with harmonic phase angle 0°. (d) PWM excitation (The duty cycle is 0.9).

Table 2. The calculation results of the two models.

	Traditional inverse model				Proposed inverse model			
	Sinusoidal		PWM		Sinusoidal		PWM	
B_p(T)	σ_1(%)	T_1 (s)	σ_2(%)	T_2 (s)	σ_3(%)	T_3 (s)	σ_4(%)	T_4 (s)
0.7	14.38	10.58	24.91	10.15	11.5	1.05	12.86	1.35
1.0	9.32	11.52	15.23	10.74	8.35	0.993	5.58	0.76
1.3	4.62	11.77	12.35	11.06	8.06	1.24	10.68	0.626

Note: σ_1-σ_4 are the errors for different conditions, and the T_1-T_4 are the corresponding computing time.

densities. However, from Fig. 7(b) to 7(d), we can find that the proposed model can well predict the asymmetric minor loops caused by harmonic and PWM excitations without measuring these situations before, which is very promising from the engineering view.

To evaluate comparative performance, both the predictive accuracy and algorithmic efficiency of the novel methodology versus the conventional approach [7] were systematically analyzed. Benchmarking protocols involved quantifying execution time requirements for 1000 sampling points per magnetic cycle, with all computational tasks executed on a standardized hardware platform featuring an Intel Core i5-7300 processor (2.50 GHz base clock). Hysteresis loop discrepancy metrics were determined via the mean absolute percentage error calculation method, formulated as:

$$\sigma = \frac{1}{N}\sum_{I=1}^{N}\left|\frac{H_{\text{meas}} - H_{\text{cal}}}{H_{\text{meas}}}\right| \times 100\% \tag{19}$$

Where H_{cal} and H_{meas} denote the computed and experimentally obtained magnetic field intensity values respectively, with N representing the total sampling points of magnetic flux density within each magnetization cycle. As tabulated in Table 2, the generalized analytical inverse Preisach framework demonstrates significantly reduced computational expenditure compared to legacy implementations, rendering it highly suitable for integration with FEM. Notably, while the proposed methodology exhibits marginally elevated error margins compared to the conventional approach under field strengths exceeding 35.58 A/m, its overall predictive accuracy across the entire flux density spectrum shows substantial enhancement for both sinusoidal and PWM excitation waveforms.

5. Conclusion

In this paper, a generalized analytical inverse Preisach model is proposed by characterizing an analytical Everett function of the irreversible magnetization component and considering magnetization-dependent hysteresis and the reversible magnetization part. Experimental evaluations confirm that the developed model maintains notable precision across both sinusoidal and non-sinusoidal excitation waveforms, and the average calculation time is much faster than the traditional method, which can be a promising candidate for coupling with the FEM-based simulations for the optimal design of electrical equipment. For future work, nonlinear surrogate models based on deep neural networks are expected to serve as promising alternatives to multi-parameter analytical models, addressing computational deviations under high magnetic flux densities.

Acknowledgment

This work was supported by the National Natural Science Foundation of China under Grant No. 52477011, 52207012.

References

[1] Y. Li and J. Zhu, J. Magn. Magn. Mater. **522**, 168655 (2022).
[2] I. Mayergoyz, Mathematical Models of Hysteresis and Their Applications. New York, Academic Press (2003) pp. 1-63.
[3] B. Vaseghi, S. A. Rahman, and A. M. Knight, IEEE Trans. Magn. **49**, 1961 (2013).
[4] E. De Biasi, J. Curiale, and R. D. Zysler, J. Magn. Magn. Mater. **419**, 580 (2016).
[5] Y. Bernard, E. Mendes, L. Santandrea, and F. Bouillault, Eur. Phys. J. Appl. Phys. **12**, 117 (2000).
[6] R. Liu, C. Gu, J. Sun, F. Shu, and B. Tang, IEEE Trans. Magn. **59**, 1 (2023).
[7] E. Dlala, J. Saitz, and A. Arkkio, IEEE Trans. Magn. **42**, 1963 (2006).
[8] S. Bi, F. Wolf, R. Lerch, and A. Sutor, IEEE Trans. Magn. **50**, 7300904 (2014).
[9] F. Vajda and E. Della Torre, IEEE Trans. Magn. **29**, 1532 (1993).
[10] P. C. Sarker, Y. Guo, and H. Y. Lu, J. Magn. Magn. Mater. **514**, 167290 (2020).
[11] S. Hussain and D. A. Lowther, IEEE Trans. Magn. **54**, 7300204 (2018).
[12] Z. Szabó and J. Füzi, J. Magn. Magn. Mater. **406**, 251 (2016).